Acoust. Sci. & Tech. **30**, 4 (2009)

INVITED REVIEW

Numerical methods for noise propagation in moving flows, with application to turbofan engines

R. Jeremy Astley*

Institute of Sound and Vibration Research, University of Southampton, United Kingdom

Abstract: This article reviews the development and application of Computational AeroAcoustics (CAA) to acoustic propagation on subsonic mean flows, with a particular focus on methods used to predict acoustic radiation from turbofan aeroengines. The governing equations are presented and particular issues such as the formulation of impedance and far field boundary conditions, the treament of Kelvin-Helmholtz instabilities, resolution requirements and methods for controlling dispersion error, are discussed. The status of current CAA methods is reviewed. Finally, the matter of validation against benchmark problems and measured data is explored.

Keywords: Computational aeroacoustics, Turbofan propagation, Aircraft noise

PACS number: 43.20.Mv, 43.20.Rz, 43.28.Js, 43.50.Lj [doi:10.1250/ast.30.227]

1. INTRODUCTION

Computational Aero-Acoustics (CAA) acquired an identity of its own in the early 1990s, defining itself as a discipline distinct and separate from Computational Fluid Dynamics (CFD). Tam wrote in 2004 [1] that CAA began 'in earnest' around ten years earlier. Many would date the birth of CAA more precisely to the publication in 1993 of the seminal article by Tam and Webb [2] which highlighted for the first time the special requirements for efficient finite difference schemes for CAA. This chronology must however be extended backwards by a decade or more if one includes more general attempts at modelling noise propagation on subsonic mean flows, particularly in relation to the noise radiated by turbofan aeroengines. Indeed, a decade or more before the term 'CAA' was coined, specialised numerical methods had been developed to model the propagation of turbomachinery noise in the ducted regions of turbofan engines. This is the starting point for the current article, and the challenge of predicting the propagation of noise from turbofan engines underpins this review. With this in mind, it is helpful to look briefly at the noise sources and propagation paths which exist in a modern High Bypass Ratio (HBR) turbofan engine.

2. SOURCES OF TURBOFAN NOISE

The accurate prediction of community noise generated by turbofan powered aircraft is a pressing requirement for noise certification of aircraft entering service. Measured data from rig and static engine tests remains the most reliable input to industry noise prediction codes, but such data are costly to acquire, and the potential benefit of using accurate CAA prediction in place of measured data is enormous.

The sources and propagation paths for noise generated in a turbofan areoengine are illustrated in Fig. 1.
The principal sources are:

- Noise generated by the fan which propagates through the intake to the forward arc, and through the bypass duct to the rear arc.
- Noise generated by the compressor which propagates into the forward arc.
- Core noise generated by the turbine and combustor which radiates in the rear arc.
- Jet noise generated by turbulent mixing in the bypass and core exhausts which forms a distributed source downstream of the engine.

Fan noise and jet noise are the dominant contributors to aircraft noise at take-off. Fan noise and airframe noise are most important at approach. Accurate prediction of fan noise is essential in both conditions.

Computational methods which are used to predict source strength will not be discussed here at any length. Correlations with measured rig and engine data play an important role in estimating turbomachinery source strengths but conventional CFD is also used to perform 'blade to blade' calculations from which the upstream and downstream acoustic modes can be extracted [3] to provide

*e-mail: rja@isvr.soton.ac.uk

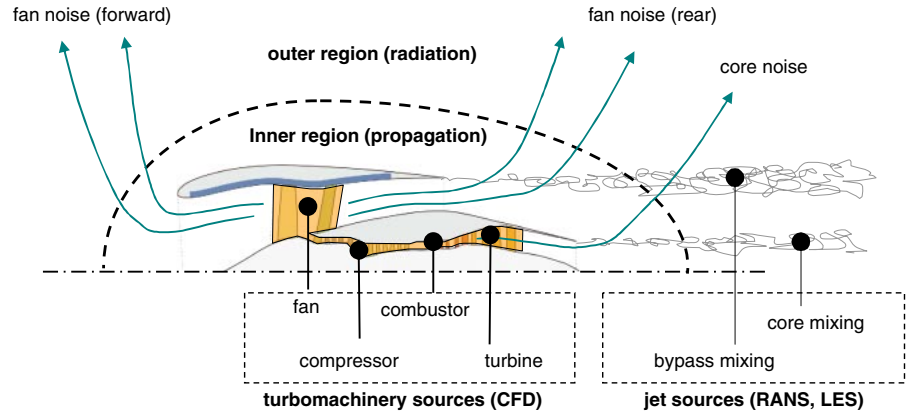

Fig. 1 Noise sources and transmission paths in a turbofan engine.

input to a propagation problem. Such calculations are often performed for a single blade passage or for a small azimuthally repeating domain which contains integer numbers of rotor and stator passages. More general arrangements of rotors and stators can however be considered by using 'chorochronic' periodicity conditions [4], and in some instances the whole rotor is modelled; in predicting low frequency buzz saw tones, for example, which depend upon small variations in blade stagger angle [5] or in performing fan flutter predictions [6]. A review of CAA/CFD methods for fan noise prediction is given in reference [7].

The other major source of noise from a turbofan engine is turbulent mixing in the jet exhaust. Hybrid methods based on Reynolds Averaged Navier Stokes (RANS) combined with the acoustic analogy are often used to model these sources, as is direct computation using Large Eddy Simulation (LES). Neither approach is relevant to the current article. A recent review of such models is given by Bodony and Lele [8].

In this article, the status of CAA methods is reviewed for noise propagation from turbomachinery sources — principally the fan — to an observer in the far field.

3. THE PROPAGATION PROBLEM

3.1. The Euler Equations

The inviscid Euler equations for a compressible fluid form the starting point for a discussion of acoustic propagation in a turbofan engine. The effects of viscosity are important only over large distances or at high frequencies, and are generally added to inviscid noise predictions in an *ad hoc* way to account where necessary for losses due to atmospheric propagation.

The full Euler equations for an inviscid, perfect gas are given by

$$\frac{\partial \rho}{\partial t} + \nabla \cdot (\rho \boldsymbol{v}) = 0, \quad \frac{D\boldsymbol{v}}{Dt} + \frac{1}{\rho}\nabla p = 0, \quad \frac{Ds}{Dt} = 0, \quad (1)$$

where ρ, p, $\boldsymbol{v}$ and s are the density, pressure, velocity and entropy respectively. The thermodynamic state variables are related by $p = \rho RT$, and entropy changes are related to pressure and density changes by; $Ds = C_v dp/p - C_p d\rho/\rho$, where C_v, C_p are the specific heats in the usual notation, and $R = C_p - C_v$.

3.2. The Linearised Euler Equations (LEE)

In the context of acoustic propagation on a mean flow, the field variables in Eqs. (1) consist of steady mean flow variables, denoted by a subscript, $_0$, and small unsteady perturbations, denoted by the superscript $'$. Eqs. (1) can then be linearised. This gives a zeroth order set of steady equations for the mean flow;

$$\nabla \cdot (\rho_0 \boldsymbol{v}_0) = 0, \quad (2)$$

$$\rho_0(\boldsymbol{v}_0 \cdot \nabla)\boldsymbol{v}_0 + \nabla p_0 = 0, \quad (3)$$

$$(\boldsymbol{v}_0 \cdot \nabla)s_0 = 0, \quad (4)$$

where $ds_0 = C_v dp_0/p_0 - C_p d\rho_0/\rho_0$. The corresponding first order equations for the perturbed quantities are;

$$\frac{\partial \rho'}{\partial t} + \nabla \cdot (\rho' \boldsymbol{v}_0 + \rho_0 \boldsymbol{v}') = 0, \quad (5)$$

$$\rho_0\left(\frac{\partial}{\partial t} + \boldsymbol{v}_0 \cdot \nabla\right)\boldsymbol{v}' + \rho_0(\boldsymbol{v}' \cdot \nabla)\boldsymbol{v}_0 + \rho'(\boldsymbol{v}_0 \cdot \nabla)\boldsymbol{v}_0 + \nabla p' = 0, \quad (6)$$

$$\left(\frac{\partial}{\partial t} + \boldsymbol{v}_0 \cdot \nabla\right)s' + \boldsymbol{v}' \cdot \nabla s_0 = 0, \quad (7)$$

where $s' = C_v(p' - c_0^2\rho')/\rho_0$, $c_0^2 = \gamma p_0/\rho_0$ and $\gamma = C_p/C_v$. After some rearrangement of terms, the linearized energy equation (7) can also be written as

$$\left(\frac{\partial}{\partial t} + \boldsymbol{v}_0 \cdot \nabla\right)p' + \boldsymbol{v}' \cdot \nabla p_0 + \gamma p_0(\nabla \cdot \boldsymbol{v}') + \gamma p'(\nabla \cdot \boldsymbol{v}_0) = 0, \quad (8)$$

in which case the linearized problem is specified by Eqs. (5), (6) and (8) with dependent variables p', ρ' and $\boldsymbol{v}'$. The same equations can also be written in conservation

form by using the momentum perturbation $(\rho \boldsymbol{v})'$ in place of $\boldsymbol{v}'$.

An important simplification occurs when the mean flow originates in a region where the temperature gradients are zero, valid for inlet flows where conditions are uniform upstream of the intake. The linearised energy equation ((7) or (8)) can then be replaced by the algebraic (homentropic) relationship

$$p' = c_0^2 \rho' \tag{9}$$

and the problem reduces to the solution of Eqs. (5) and (6) for a reduced set of variables (ρ' *or* p', and $\boldsymbol{v}'$).

A further simplification is possible when the mean flow is irrotational. The perturbed velocity can then be written in terms of an acoustic velocity potential $\phi'(\boldsymbol{x}, t)$ and the linearised momentum equation is replaced by an unsteady form of Bernoulli's equation;

$$\frac{p'}{\rho_0} = \frac{c_0^2}{\rho_0}\rho' = -\left(\frac{\partial}{\partial t} + \boldsymbol{v}_0 \cdot \nabla\right)\phi'. \tag{10}$$

After some rearrangement of terms, the continuity equation can be re-written as a convected wave equation

$$\frac{D}{Dt}\left(\frac{\rho_0}{c_0^2}\frac{D\phi'}{Dt}\right) - \nabla \cdot (\rho_0 \nabla \phi') = 0. \tag{11}$$

Equation (11) has been derived here by assuming irrotational flow. Pierce [9] has shown however that it holds also for acoustic propagation on arbitrary unsteady flows provided that the wavelength is sufficiently small.

To summarize: In the most general case the linear propagation problem involves the solution of five Eqs. (5–7, 8) for five variables, p', ρ' and $\boldsymbol{v}'$. The number of variables reduces to four in the case of homentropic flow when Eq. (7) is replaced by expression (9). When the mean flow is irrotational, the problem reduces to the solution of Eq. (11) for a single unknown parameter, the velocity potential ϕ'.

Time-harmonic versions of these problems are obtained by rewriting each dependent variable, $q'(\boldsymbol{x}, t)$ say, in terms of a complex amplitude $\tilde{\boldsymbol{q}}(\boldsymbol{x})$ where

$$q'(\boldsymbol{x}, t) = Re(\tilde{\boldsymbol{q}}(\boldsymbol{x})e^{i\omega t}) \tag{12}$$

and by replacing the operator $(\partial/\partial t)$ by $(i\omega)$. For example, the time-domain velocity potential formulation (11) transforms to a convected Helmholtz equation;

$$(i\omega + \boldsymbol{v}_0 \cdot \nabla)\left[\frac{\rho_0}{c_0^2}(i\omega + \boldsymbol{v}_0 \cdot \nabla)\tilde{\boldsymbol{\phi}}\right] - \nabla \cdot (\rho_0 \nabla \tilde{\boldsymbol{\phi}}) = 0. \tag{13}$$

For the case of zero mean flow, this reduces to the well-known Helmholtz equation for a stationary medium

$$\nabla^2 \tilde{\boldsymbol{\phi}} + k_0^2 \tilde{\boldsymbol{\phi}} = 0, \tag{14}$$

where $k_0 = \omega/c_0$. Note that in the case of Eqs. (11) and (13) the unsteady pressure can be recovered from the velocity potential solution by using expression (10) or its frequency domain equivalent.

3.3. Acoustic, Vorticity and Entropy Modes

Local solutions exist for Eqs. (5–7, 8) for the case of uniform mean flow. These are helpful in understanding the nature of the unsteady disturbance. A local wavelike disturbance of the form;

$$\boldsymbol{q} = \bar{\boldsymbol{q}} e^{i(\omega t - k_x x - k_y y - k_z z)} \tag{15}$$

where $\boldsymbol{q} = [\rho', u_x', u_y', u_z', p']^{\mathrm{T}}$, is a solution for the case $\boldsymbol{v}_0 = (U_0, 0, 0)$ — uniform flow in the x direction — provided that ω and $\boldsymbol{k} = (k_x, k_y, k_z)$ satisfy one of three distinct dispersion relationships [2]. These correspond to three types of disturbance;

- *Entropy waves*. These have a dispersion relationship,

$$\omega = U_0 k_x, \tag{16}$$

  and the solution vector $\boldsymbol{q}$ contains no pressure or velocity components. These solutions are density fluctuations which are convected with the mean flow.
- *Vorticity waves*. These satisfy the same dispersion relationship (16) as entropy waves but contain no density or pressure components. They are vortical disturbances which convect with the mean flow.
- *Acoustical waves*. These satisfy the dispersion relationship;

$$(\omega - U_0 k_x) = \pm c_0 |\boldsymbol{k}|. \tag{17}$$

  All of the physical variables are present in the solution vector $\boldsymbol{q}$. These solutions are acoustical disturbances which propagate with phase speed c_0 in a frame of reference fixed in the moving fluid.

All three modes are present in general solutions of Eqs. (5–7, 8). They do not interact when the mean flow is uniform, but couple when shear flow is present, and at boundaries. Also the entropy mode does not exist for the homentropic case when the energy equation is replaced by Eq. (9). Neither the entropy nor the vorticity mode is supported by the irrotational formulation (Eqs. (11) and (13)).

3.4. The Computational Domain

The geometry of a typical intake problem is illustrated in Fig. 2. An exhaust model is similar in appearance except that the nacelle lip is replaced by the exhaust nozzle and the flow direction is reversed. We assume that the equations are solved on a finite computational domain R, bounded by a far field truncation boundary S_∞. The fan noise source is specified on source plane S_s. A locally reacting impedance $z(\omega)$ is defined on an impedance surface S_z. S'_∞ is an integral surface within R used to define the far-field solution.

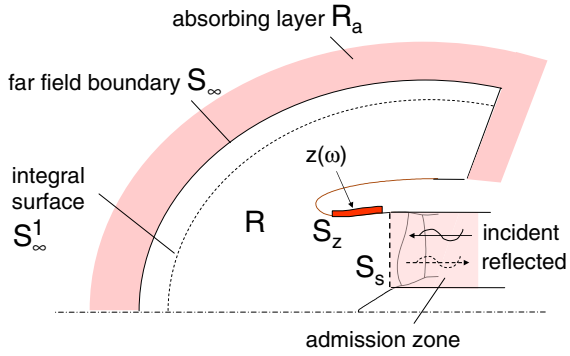

Fig. 2 Geometry of an intake problem. R is the computational domain.

3.5. The Impedance Boundary Condition

The performance of acoustic liners is usually specified in terms of a complex normal impedance $z(\omega)$. This defines the relationship between the complex pressure and the complex velocity normal to the surface;

$$z(\omega) = \frac{\tilde{p}}{\tilde{\boldsymbol{v}} \cdot \boldsymbol{n}} \quad \text{or} \quad \tilde{p} = z(\omega)\tilde{\boldsymbol{v}} \cdot \boldsymbol{n}, \tag{18}$$

where $\boldsymbol{n}$ is a unit normal into the surface. When grazing flow is present, this condition must be projected through the boundary layer (bl). It is commonly assumed that pressure and particle displacement are continuous across the bl. This is the basis for the widely used 'Myers' boundary condition [10]

$$\tilde{\boldsymbol{v}} \cdot \boldsymbol{n} = \frac{\tilde{p}}{z(\omega)} + \boldsymbol{v}_0 \cdot \nabla\left(\frac{\tilde{p}}{i\omega z(\omega)}\right) - \frac{\tilde{p}}{i\omega z(\omega)} \boldsymbol{n} \cdot (\boldsymbol{n} \cdot \nabla \boldsymbol{v}_0). \tag{19}$$

The second term on the Right Hand Side (RHS) represents the convective effect of the grazing flow; the third term is associated with the curvature of surface. The RHS of Eq. (19) includes a tangential derivative of impedance. This causes problems of implementation when there is a step change in impedance (from a lined to a hard-walled segment for example). Eversman [11] has rearranged the Myers condition in a way which largely removes this problem. While the Myers/Eversman boundary condition is used in many current numerical models, debate persists on whether continuity of particle displacement is the appropriate condition to apply, and whether the Myers condition deals correctly with hydrodynamic modes in the boundary layer [12,13].

Time-domain versions of Eqs. (18) and (19) are needed for CAA formulations in the time domain. In theory Eq. (18) can be re-written in the time domain by taking an inverse Fourier transform to give

$$p'(\boldsymbol{x}, t) = \frac{1}{2\pi} \int_{-\infty}^{\infty} z'(\boldsymbol{x}, t-\tau) v_n'(\boldsymbol{x}, \tau) d\tau, \tag{20}$$

where $z'(t)$ is the inverse fourier transform of $z(\omega)$. Equation (20) must then be combined with the Myers condition. However, any evaluation of expression (20) poses problems in practice. First, $z(\omega)$ is generally defined over a limited frequency range on the real axis, and must be extrapolated over the complex plane if $z'(t)$ is to be defined. Moreover, this must be done in such a way that the problem remains causal, the variables real and the wall passive [14]. Also the time history of the normal velocity, $v_n'(\boldsymbol{x}, t)$, must be stored indefinitely if the convolution integral is to be evaluated at each time step.

A number of time-domain impedance models have been proposed which do not involve the evaluation of expression (20). These include the model of Tam and Auriault [15], and related approaches [16], and the z-transform method of Özyörük and Long [17]. Both have been widely applied. Tam's method uses a mass-spring-damper model to represent the behaviour of the liner. In Özyörük's method two steps are required; first the impedance data must be fitted to a rational continuous model which is inherently stable, and then a z-transform is used to define a local approximation to Eq. (20). An interesting third approach introduces additional degrees of freedom in the numerical model which physically model propagation in a Helmholtz resonator attached to each computational cell on the boundary [18]. All of the above approaches give reasonable results for attenuation in test ducts with subsonic mean flow. There are however unresolved issues in practice associated with stability, and specifically with the status of Kelvin-Helmholtz-type instabilities when there is a slip condition at the wall. These are often filtered numerically in time-domain numerical schemes, but there is ongoing debate as to whether this is an appropriate treatment [14,20]. A comprehensive review of time-domain impedance boundary conditions is presented by Fung [19].

3.6. The Far Field Boundary Condition

At the far field boundary S_∞ of Fig. 2, the numerical solution must leave the computational domain R without spurious reflection. Three approaches are commonly used.

3.6.1. Characteristic boundary conditions

These are derived by writing the equations on the boundary in characteristic form and assigning values to incoming characteristic quantities [21–23]. The approach is widely used, and performs well when the outgoing wave is normal to the grid boundary. A review of such methods is given by Hixon [24].

3.6.2. Asymptotic boundary conditions

These are based on prior knowledge of the asymptotic form of the solution at large distances from the source. For the acoustical modes the simplest such condition is the 'ρc' impedance, or its Lorentz transformed equivalent with

mean flow. This can be regarded as a 'zeroth order' condition approximating the Sommerfeld radiation condition. This can be improved by taking into account geometric spreading as $r^{-1/2}$ or r^{-1} for 2D and 3D problems respectively. An 'order 1' boundary condition of this type is formulated by Tam and Webb [2] for the acoustic portion of the solution, along with compatible boundary conditions which enforce the correct behaviour for the entropy and vorticity modes at inflow and outflow boundaries. The disadvantage of asymptotic boundary conditions of low order is that they work most effectively only at large distances from the source. The higher the order of the boundary condition, however, the closer the 'infinite' boundary S_∞ can be placed to the source. High order Infinite Elements [25,26] exploit this by defining an unbounded computational domain, beyond S_∞, in which the numerical solution is based on a high order, uniformly convergent asymptotic expansion for the radiated field [27]. In this sense the infinite elements act as a high order asymptotic boundary condition to the solution in R. This has proved robust in practice and is implemented in the NASA 'Eversman' code and in the commercial CAA code 'ACTRAN/TM' [28]. A time domain implementation of this approach has also been demonstrated [29].

3.6.3. Zonal methods

A third approach to terminating the computational domain in the far field is to extend the computational region to include an absorbing (or 'buffer') zone beyond S_∞, the region R_a in Fig. 2. The solution in this zone is non-physical, but is damped either explicitly by a low pass filter, or implicitly by grid stretching, or by the the addition of extra terms in the equations which damp the solution as is propagates normal to the boundary. Such methods are reviewed by Hu [30]. A variant on the 'absorbing' zone is the 'Perfectly matched Layer' (PML), a concept proposed initially by Berenger [31]. An up-to-date review of the PML as applied to CAA is given by Goodrich [32] who compares the effectiveness of three different PML implementations. The important distinction between the PML and the conventional absorbing layer is that in theory disturbances entering the PML experience no reflection at S_∞ irrespective of wave angle, and are then damped within the layer in all directions. A careful comparison of an explicit absorbing layer, several implicit absorbing schemes, and a PML based on the popular formulation of Hu [33] is presented by Richards [34]. This indicates that the buffer zone with explicit damping performed the best, and was the simplest method to implement, giving excellent results when the zone depth was of the order of one wavelength or greater.

While the discussion above has been of damping *all* disturbances at the far field boundary, zone methods can equally be used to impose a specified incoming wave field at a source boundary [30,34]. This is done by dividing the solution in an admission zone (see Fig. 2) into (known) incident and (unknown) reflected parts and by applying the zonal damping only to the reflected part.

3.7. Kelvin-Helmholtz (KH) Instability

An infinitely thin shear layer in an inviscid flow is unstable according to classical theory of Kelvin and Helmholtz [35]. For a shear layer of *finite* thickness, however, excited at a specific frequency, unstable spatial modes exist only if the shear layer thickness is sufficiently thin compared to a hydrodynamic lengthscale (u_0/ω) [36]. In practice some portions of the exhaust shear layers close to the nozzle will be unstable and the growth of such instabilities destabilizes LEE computations. In the real flow such modes will not grow indefinitely but will be attenuated and controlled by viscous and non-linear effects. Since these are absent in the linearized equations it is debatable whether such numerical instabilities are 'physical' or not. In the framework of the LEE however they are part of the numerical solution and this poses a practical issue in application to exhaust flows. In many instances the mixing layers grow sufficiently rapidly for the growth of the KH instabilities to be controlled by this spreading effect. Time-domain LEE solvers then produce solutions which are globally stable but in which the 'instabilities' are present where the mixing layer is thin [37]. An absolute guarantee that the LEE solution will not be destabilized by KH instabilities is however more difficult to achieve.

One option is to solve the LEE in the frequency domain. It is known that a correctly posed solution of the time harmonic equations cannot support KH instabilities. A direct solver must however be used to solve the resulting discrete equations since the use of an iterative solver is analogous to marching forward in time [38]. This is a serious constraint however on problem size.

Alternatively the time-domain LEE can be modified to suppress the instabilities. Various methods have been used. The LEE can be formulated for example with additional non-physical nonlinear terms designed to control any instable modes [39]. Another technique is to selectively remove the terms in the time domain LEE which cause the instabilities (for parallel flow in the x direction these are terms involving mean flow gradients $\partial u_0/\partial y$, and $\partial u_0/\partial z$) [40]. A more recent variant which automatically ensures that the equations are modified so that all non-acoustic modes are suppressed is to use the Acoustic Perturbation Equations (APE), as formulated by Ewert and Schroder [41]. APE has recently been implemented by Huang [42] for turbofan exhaust flows and shown to give solutions that are similar to those obtained by removing explicitly the flow gradient terms. All of these methods produce sensible solutions but there is ongoing debate as to whether

removing or modifying terms in the equations changes significantly the acoustic solution. In a recent article Tester *et al.* [43] have investigated this matter by solving the LEE in the frequency domain with and without suppressing the gradient terms. These studies indicate that for realistic exhaust nozzles inclusion of the gradient terms has an observable but small effect in the far field (of the order of 1–2 dB at most in Sound Pressure Level (SPL)).

3.8. Reconstruction of the Far Field

None of the far field boundary treatments described previously, except for the infinite element method, predicts directly the far field sound pressure level. The far field SPL is obtained in most cases by extracting computed time pressure histories (or complex amplitudes in the time-harmonic case) on a surface S'_∞ which lies within the computational domain, and using these values within an integral formulation to project the solution to the far field. The Kirchhoff integral formulation [44], or Farassat's version 1A of the Ffowcs Williams and Hawkings (FWH) equation are commonly used [45]. The FWH equation has the advantage that the mean flow need not have reached a uniform state for the integral formulation to be valid.

4. RESOLUTION REQUIREMENTS AND DISPERSION ERROR

The characteristic wavelength of an acoustic disturbance in a turbofan engine at frequencies of practical interest, is generally an order of magnitude smaller than a reference geometric lengthscale, typically the outer fan diameter. This is one of several multiscale challenges faced by CAA [1] and has a strong influence on grid generation. In simple terms, an effective CAA scheme must propagate the acoustic solution over many wavelengths without incurring cumulative numerical errors through dissipation or dispersion. Such schemes must therefore be *extremely* accurate over a single wavelength. The error in the numerical solution can be characterised as an amplitude (dissipation) error and a phase (dispersion) error. The dispersion error is particularly important for acoustic problems since a small, say 1%, phase error over a single wavelength will result in a complete reversal of phase over a propagation path of 50 wavelengths. The importance of controlling dispersion error in numerical schemes for aeroacoustics and the unsatisfactory nature of conventional low order CFD in this respect was first highlighted by Tam [2] and has since become a standard consideration in the development of CAA methods [46]. Tam observed that traditional finite-difference interpolation was inherently poor at representing periodic spatial solutions. By using a simple approximability argument, he showed that an effective wavenumber k' could be derived which is characteristic of particular numerical stencil. This represented the best numerical approximation that can be achieved for a spatial wavenumber k. The parameter $k'\Delta x$ where Δx is the spacing between grid points is proportional to the number of grid points per wavelength, with $k'\Delta x = \pi$ representing the spectral limit of two points per wavelength. Values of $k'\Delta x$ are plotted against $k\Delta x$ in Fig. 3 for various CAA schemes. The diagonal line represents a perfect solution free of numerical error. Values of $k\Delta x$ corresponding to 5 and 10 grid points per wavelength are also indicated. In the same article, Tam proposed a number of new Dispersion Relation Preserving (DRP) CAA schemes in which the stencil coefficients were specifically chosen to reduce the error in k'. Data for Tam's fourth order DRP scheme are plotted in Fig. 3 and compared to standard 2nd and 4th order central difference schemes. Also shown are data for two 4th order prefactored compact schemes designed by Ashcroft and Zhang [46] to minimise dispersion error.

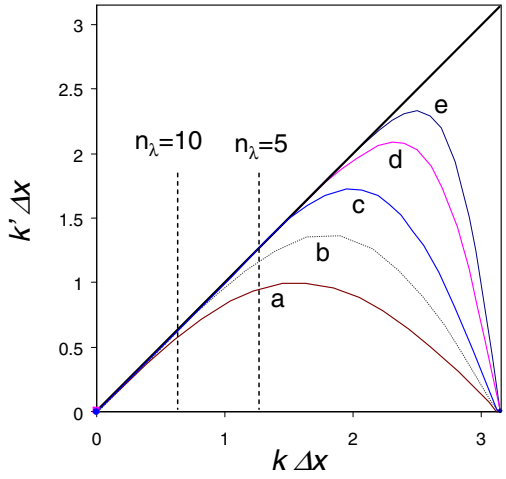

Fig. 3 Dispersive characteristics of CAA schemes. (a) 2nd order central diff. (b) 4th order central difference. (c) 4th order DRP [2]. (d) 4th order optimized compact (3 point stencil) [46]. (e) 4th order optimized compact (5 point stencil) [46]. n_λ is the number of points per wavelength.

Two points are clear from the data in Fig. 3. Firstly, high order methods of any description reduce dispersion error and offer a very significant improvement over traditional 2nd order CFD. Secondly, optimized schemes such as Tam's DRP scheme, and Ashcroft's optimized compact schemes offer further improvements over conventional schemes of the same order. In Ref. [46] for example the authors show that by using schemes (d) and (e) of Fig. 3, a 0.5% dispersion error over a single wavelength can be achieved by using 5 and 4 grid points per wavelength respectively. To achieve the same accuracy on a conventional 2nd order mesh, 63 grid point per wavelength are required. The implications for turbofan

propagation problems are profound. Noise predictions are generally required for frequencies up to 10 kHz, though it is often possible to extrapolate numerical solutions at the upper end of this range by using high frequency approximations. However, if we assume that predictions are needed for frequencies up to say 3 kHz, the acoustic wavelength at this frequency is of the order of 0.1 m. The near field mesh in region R of Fig. 3 must however extend at least one fan radius beyond the nacelle itself. For a typical fan diameter of say 2 m, the physical size of the meshed region R is then in excess of say $20\,m^2$ for an axisymmetric model, and $100\,m^3$ for a three-dimensional model. A high order mesh, based on 7–10 grid points per wavelength, would then contain in excess of 100,000 grid points for an axisymmetric model, and 30 million grid points for a full three-dimensional model. If a conventional 2nd order method were used, the 'points per wavelength' requirement would increase by an order of magnitude, and the total number of points by two and three orders of magnitude respectively. The necessity of using high order methods to bring the required number of grid points within reasonable bounds is self evident.

5. THE STATUS OF CURRENT METHODS

CAA methods currently applied to turbofan propagation will be reviewed in this section. They are presented roughly in order of increasing generality and complexity.

5.1. Boundary Element Methods

The Boundary Element Method (BEM) is the computational method of choice for many acoustic applications in the absence of flow [47]. It requires a surface rather than a volume discretization and generates a smaller, though less sparse, set of discrete equations compared to a domain-based method. It is less well suited to flow acoustics since an analytic Green's function is required and this is available only for uniform flow. The BEM was used in early computational models for turbofan acoustics by coupling it iteratively to finite elements in the near field [48]. More recently Dunn, *et al.* [49] presented a Boundary Integral approach to modelling propagation and radiation of forward and rear arc noise from a thin walled, lined cylindrical duct with uniform flow and a turbofan-like source. While the BEM clearly does not represent the flow physics fully, because of the assumption of uniform flow, it is nonetheless a valuable approximate tool which can be applied to fully three-dimensional intakes at acceptable cost, and has been used for this purpose in recent years [50,51]. Interest in the use of BEM for such calculations has increased with improvements in performance through the use of Fast Multipole Methods (FMM), implemented for example in the EADS/AIRBUS BE code actipole [52,53].

5.2. The Parabolic Equation Method

The parabolic approximation to the wave equation has been used extensively in underwater acoustics and is based on a wave splitting approach in which the scheme marches 'forward' from the source to the receiver and neglects backward reflections. It is very fast for this reason and deals well with three-dimensional problems. Against this must be balanced the knowledge that it will give poor results when reflections and backscattering are present. The method was implemented for nacelle calculation by Boeing in the late 1990s [54] and has been maintained and further developed by NASA since then as the nacelle prediction code CDUCT-LaRC [55,56].

5.3. Finite Element Helmholtz Methods

The use of finite elements in the frequency-domain for flow acoustic propagation dates back to the early 1980s. Such schemes solve the convected Helmholtz problem of Eq. (13) on an irrotational mean flow. The 'Eversman' code based on the formulation developed by Astley, Eversman and others almost three decades ago [57–59] is typical of this aproach. Quadratic finite elements are coupled to infinite elements which act both as a non-reflecting boundary and as a far field pressure representation. In the context of Fig. 3 the scheme is 4th order accurate [60]. Some directional effects are evident in two and three dimensions when the mean flow is aligned with the mesh [61]. The fan source is represented by a modal expansion on the fan plane. An improved version of the Astley-Eversman formulation which uses mapped infinite elements in place of the original wave envelope elements [26] was developed in the late 1990s, and the same formulation is implemented in the commercial code ACTRAN/TM [28]. Similar schemes which use high order spectral elements have also been developed [62], though using an absorbing layer rather than an infinite element termination. Higher order Lagrangian elements have also been shown to give improved accuracy [63] but are not as simple to mesh and are not widely used. The Eversman code is formulated for an axisymmetric domain but permits an acoustic field which varies as $e^{im\theta}$, where θ is an azimuthal angle about the geometric axis of symmetry, commonly referred to as a '2.5D' model. ACTRAN/TM is implemented for both axisymmetric and 3D problems [28].

The Finite Element/Infinite Element approach has several advantages. It is unstructured which makes automatic mesh generation relatively simple, and has the dispersion characteristics of a fourth order scheme when quadratic elements are used. At the time of writing, it is the only CAA tool which is commercially available and routinely used in industry. The disadvantages of the method are that it requires a direct solver which means that solution time scales steeply with problem size, and it is

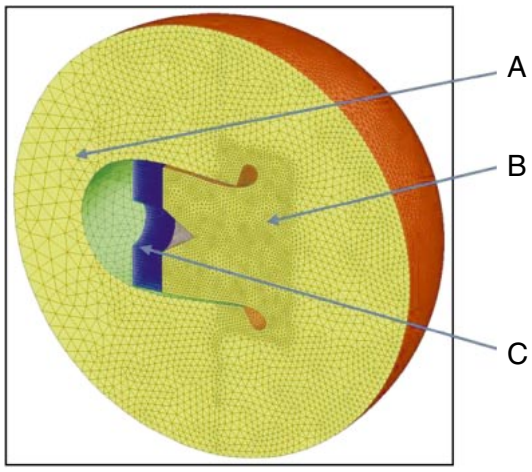

Fig. 4 Actran/TM FE/IE mesh for an analysis of a bellmouth intake (see [28]) indicating varying mesh resolution. Region A: Low resolution mesh in rear arc. B: high resolution mesh required for region of high velocities and high velocity gradients. C: Nominal 'fan plane' for modal source definition.

restricted to irrotational flows, which precludes its straightforward use for exhaust propagation. The latter objection can be partially overcome by the introduction of vortex sheets to approximate a mixing layer. Matching the pressure and particle velocity across such a discontinuity captures much of the physics of the problem [64]. The more fundamental problem of solving large linear systems by using direct solution methods at an acceptable computational cost has been partially alleviated by the use of 64 bit processors, able to access large quantities of memory, along with significant algorithmic improvements in parallel direct frontal solvers such as MUMPS [65]. As an indication of the current capabilities and limitations of this approach, a three-dimensional ACTRAN/TM mesh for the bellmouth intake of a CF34-8E/Embraer nacelle is shown in Fig. 4. This model is discussed in detail in [28]. Single frequency analyses can be performed for frequencies corresponding to values of kR between 40 and 45. Four threads on a single Intel Xeon 3.0 GHz node are used. The CPU time is about 2 hours for each frequency. Figure 4 also illustrates the advantage of an unstructured mesh in which the resolution of specific areas (region B, for example) can be increased without driving up grid resolution elsewhere.

5.4. Structured Methods for LEE

Two approaches are commonly used to solve the LEE on structured grids. These are the DRP scheme of Tam and Webb [2] and the low dispersion compact schemes of Ashcroft and Zhang [46]. Both methods lend themselves to efficient parallelization when implemented in the time domain. The DRP scheme, has been on the scene longest. It forms the basis for many CAA research [67] and in-house industry codes [66]. Some of these are able to solve large 3D turbofan problems at realistic frequencies [68]. The DRP idea also forms the basis for variants such as the high order optimised upwind scheme of Zhuang [69] and a high order DRP base finite volume approach [70].

DRP implementations are predominantly in the time-domain, where the potential for efficient parallelization is greatest. High order 'DRP-like,' finite difference schemes have also been implemented however in the frequency-domain. An important example is the FLESTURN code implemented by Özyörük [71] for 2.5D intake and exhaust problems. This uses the MUMPS direct solver.

High order, optimised, prefactored compact schemes have also been widely used for CAA propagation. They provide an alternative structured approach and have the advantage of reducing the stencil size and facilitating the formulation of stable stencils near boundaries. A family of high order accurate compact schemes with low dissipation and dispersion was proposed by Ashcroft and Zhang [46], extending earlier work by Hixon [72]. Dispersion data for fourth order schemes of this type with three and five point stencils are included in Fig. 3. Such schemes have been applied to intake and exhaust problems in 2.5D and in 3D [34,73–76].

Structured meshes are generally regarded as a disadvantage from the point of view of mesh generation. The use of overlapping ('chimera') grids provide a partial solution to this problem. This approach has been adopted in the TUBA DRP codes developed by Schoenwald, Thiele and others [67]. A chimera grid for a scarfed intake is shown in Fig. 5. Adaptive mesh refinement has also been used to achieve nonuniform mesh resolution for a DRP computation on block structured grids [77].

The computational demands of DRP and compact schemes are comparable, and both can exploit very high parallel efficiencies. In terms of the overall computational effort required for turbofan applications, the CPU time for the 3D exhaust analysis of ref [76] performed using the sixth order accurate compact scheme of ref [46] is 40 hours running in parallel on a cluster of 12, 3.06 GHz processors. The Helmholtz number kR is 28. This is more demanding in terms of CPU than the figure quoted for the ACTRAN/TM intake solution of comparable size noted in the previous section, but also less memory intensive and more easily scalable with the number of processors.

5.5. Unstructured Methods for LEE

The practical advantages of unstructured grids are well known for industrial applications, and indeed the method of choice for industrial CFD is to use low order schemes on unstructured grids. The implementation of higher order CAA methods on unstructured grids is not straightforward.

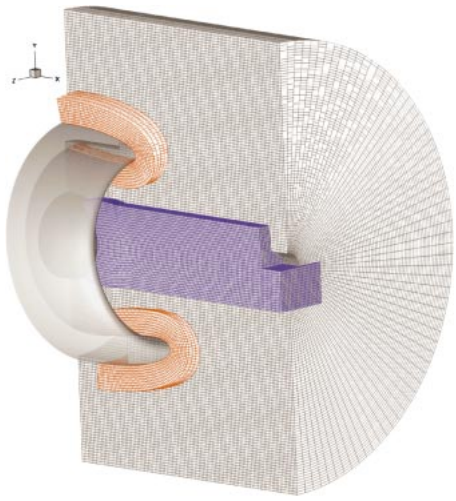

Fig. 5 Chimera grid for DRP analyis of a three-dimensional intake showing overset grid used to represent the nacelle lip geometry [67].

Kok [70] has proposed a high order DRP extension of a finite volume scheme, although implemented on a structured grid. The most promising high order unstructured scheme for the LEE is the Discontinuous Galerkin Method (DGM) [78], a flux based finite element approach which allows variable orders of approximation within irregularly shaped elements.

A number of DGM schemes have been proposed for the LEE [79–83] and studies performed to assess their accuracy and stability [84,85]. In terms of practical application to turbofan acoustics, the ACTRAN/DGM code [83] developed in the MESSIAEN and TURNEX projects funded by the European Union under the sixth framework programme (FP6) is probably the most advanced. The performance of this code for 2.5D and 3D exhaust problems is generally comparable to that of structured schemes [86]. For example, a realistic model of a 3D exhaust problem with 27 million degrees of freedom at a frequency corresponding to $kR = 30.0$ executes in 24 hours on 16 processors. The method scales well with frequency and the same problem at $kR = 70$ runs on the same system in 4 days.

While the strengths of the DGM formulation lie predominantly in the time domain, it has also been implemented in the frequency domain to circumvent the problems associated with Kelvin Helmholtz instabilities [87].

5.6. Solution of the Full Euler Equations

The use of the full — rather than the linearized — Euler formulation for CAA has the advantage that Kelvin Helmholtz instabilities are damped 'naturally' by nonlinear terms. Such schemes can also accommodate nonlinear propagation effects close to the fan and the formation of shocks. The sAabrinA code [88] developed at ONERA is an example of a scheme of this type. The full Euler equations are solved with sixth order spatial accuracy and high order time integration. The application of sAbrinA to a realistic 3D engine exhaust including pylon effects is presented in [88]. A computation over 17.55 periods of the source excitation for $kR = 29.8$ required 55 CPU hours, though it is not clear on what system the computation was performed. Nonetheless, this indicates that the overhead of using full Euler rather than LEE may not be excessive.

5.7. Physics Based Methods

The unsuitability of polynomial bases for representing spatially periodic wavefields lies at the heart of the dispersion and resolution requirements of most CAA codes. Numerical methods which use basis functions which are themselves 'wavelike' have been studied as a potential remedy for this problem. Casalino [89] has proposed a Green's function approach for the solution of Eq. (13) for propagation on irrotational flow. A finite difference stencil is formulated which is consistent with a superposition of Green's function sources at grid points. Since these are local solutions of the governing equations, the dispersion characteristics of the scheme are excellent and grid spacing can extend over several wavelengths.

A similar philosophy underpins the Partition of Unity approach applied to the same equations by Gamallo and Astley [90] in which a local basis of plane waves is used within a conventional finite element formulation. Again, elements can be used which extend over several wavelengths permitting very coarse meshes and reducing the overall size of the discrete problem. The accuracy of the method is however limited by conditioning. More recently, a wave-based discontinuous Galerkin approach has been applied by Gabard [91] to the frequency-domain LEE, in which acoustic, vorticity and entropy waves are present in the element bases and fluxes.

6. VALIDATION AND BENCHMARKING

The methods reviewed in this article can be assessed by comparing computed solutions to known analytic solutions; by testing for consistency between different methods when applied to problems for which no exact solution exists; and by comparing to measured data.

Most of the methods described in previous sections have been benchmarked against analytic solutions such as those of Homicz and Lordi [92], Munt [93] or Gabard [94]. These give an idealised model for propagation from an intake or exhaust. In each case a mode radiates from the open end of a circular or annular pipe, propagating with or against a mean flow. The problem of Homicz and Lordi [92] is shown in Fig. 6. In the case of the Munt solution a cylindrical vortex sheet exists downstream of the exhaust

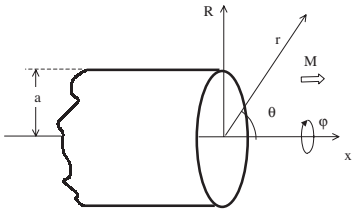

Fig. 6 Homicz and Lordi benchmark problem [92].

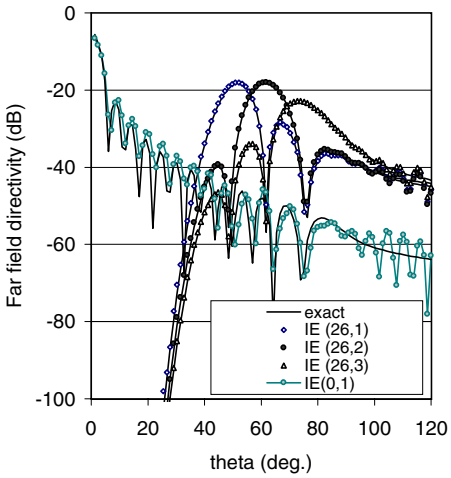

Fig. 7 Comparison of exact and computed far field directivities, Homicz and Lordi benchmark problem. $M = -0.5$, $ka = 35$. Modes (26,1), (26,2), (26,3) and (0,1) incident. Computed solution, FE/IE Helmholtz model [95]. θ is the polar angle as shown in Fig. 6.

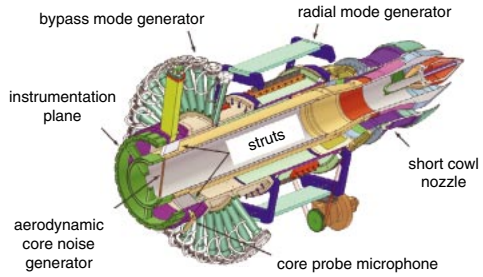

Fig. 8 TURNEX short cowl exhaust rig [96].

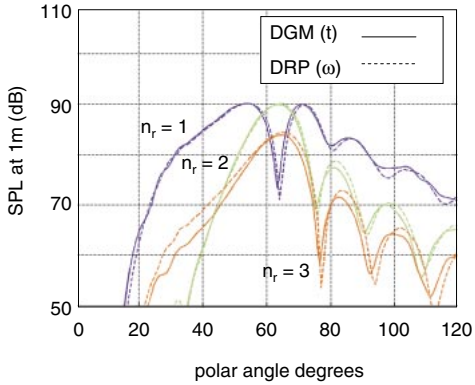

Fig. 9 Far field SPL directivity scaled to 1 m radius for short cowl TURNEX exhaust rig. Azimuthal mode order; $m = 10$. Comparison of CAA predictions for time domain DGM and frequency domain DRP [96].

lip. A comparison of analytic and predicted far field sound directivities for the Homicz and Lordi problem is shown in Fig. 7. The computed solution is obtained by using a Helmhholtz, frequency-domain Finite and Infinite element model [95]. Similar comparisons have been made and similar correspondence achieved for structured and unstructured LEE codes.

Direct comparisons between different CAA codes applied to the same problem are less common, and comparisons to measured data extremely rare. Comprehensive comparisons of both type were recently performed in the TURNEX project funded by the European Commission, and some of this data is available in the public domain [96]. The TURNEX project included rig scale tests of geometrically realistic, short cowl and long cowl, coaxial exhausts. Spinning modes were generated in the bypass duct by a mode synthesiser, and propagated through the jet shear layer into a large anechoic jet test facility. Far field SPL measurements were taken using polar and azimuthal microphone arrays. A rotating microphone array in the bypass duct down stream of the synthesiser decomposed the source field into azimuthal and radial orders. The rig is illustrated in Fig. 8.

A number of CAA codes were used to predict the sound field in the rear arc. At each frequency, the incident power of each mode was determined from the modal decomposition in the bypass duct. A comparison of far field SPL — referenced to a nominal 1 m radius — is shown in Fig. 9. Results are shown for the short cowl engine for an azimuthal mode order $m = 10$ and for a frequency characteristic of Blade Passing Frequency (BPF) at approach. The mean flow is also typical of the approach condition. Results are shown for two prediction schemes, a time domain DGM code (ACTRAN/DGM) and a frequency-domain DRP scheme (FLESTURN). Results are presented for each radial mode and plotted against polar angle measured from the axis of the exhaust. Slight differences can be observed between the two predictions but on the whole, the correspondence between the predictions of the two schemes acts to validate both for engineering purposes.

Finally, a comparison of predicted and measured data for the same rig is shown in Fig. 10. The prediction is from the FLESTURN DRP code but a similar prediction using the time-domain DGM scheme — not shown here — is virtually indistinguishable. Measured data from the polar and azimuthal arrays are labelled as measurement (a) and measurement (b). Notwithstanding some scatter in the data,

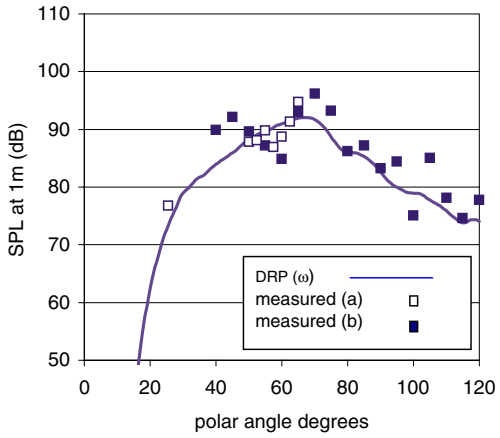

Fig. 10 Far field SPL directivity scaled to 1 m radius for short cowl TURNEX exhaust rig. Azimuthal mode order $m = 10$. Comparison of CAA predictions with measured data [96].

the correspondence with the predicted result is encouraging. It should be noted that the comparison is made without any normalization or adjustment of the far field levels. These are absolute predictions based on the measured source amplitudes.

7. CONCLUSIONS

The current state of CAA for turbofan noise propagation has been reviewed. The use of CAA in this important application has advanced greatly over the last decade. Linearised models based on the potential wave equation and LEE are able now to deal relatively easily with axisymmetric geometries. Predictions obtained using such models are beginning to find their way into industry prediction procedures. The solution of 3D problems is more challenging, but solution times are approaching values which would be regarded as acceptable to engine manufacturers and airframers (turnaround times measured in hours rather than days). Indeed robust commercial Helmholtz codes are already quite widely used for intake and in-duct bypass duct noise prediction. Structured and unstructured time-domain LEE codes are however more suitable for exhaust computations. A number of techniques have been proposed to deal with Kelvin-Helmholtz instabilities which historically have impeded the progress of such computations. The acoustic perturbation equations may also offer a systematic way of dealing with this issue. Comparisons between the mainstream CAA propagation methods indicate that they generate results which are consistent with each other, within the limits of slightly different assumptions which are made. The scarcity of non-proprietary data makes it difficult to assert at this stage that current CAA predictions correctly predict the noise which is actually radiated from turbofan engines, but the comparisons of this type which exist are encouraging.

REFERENCES

[1] C. K. W. Tam, "Computational aeroacoustics: An overview of computational challenges and applications," *Int. J. Comput. Fluid Dyn.*, **18**, 547–567 (2004).

[2] C. K. W. Tam and J. C. Webb, "Dispersion-relation-preserving finite difference schemes for computational acoustics," *J. Comput. Phys.*, **107**, 262–281 (1993).

[3] A. G. Wilson, "Application of CFD to wake/aerofoil interaction noise — A flat plate validation case," *AIAA Paper 2001-2135* (2001).

[4] G. A. Gerolymos, G. J. Michon and J. Neubauer, "Analysis and application of chorochronic periodicity in turbomachinery rotor/stator interaction computations," *J. Propul. Power*, **18**, 1139–1152 (2002).

[5] M. J. Wilson, M. Imregun and A. I. Sayma, "The effect of stagger variability in gas turbine fan assemblies," *ASME J. Turbomach.*, **129**, 404–411 (2007).

[6] X. Wu, M. Vahdati, A. I. Sayma and M. Imregun, "Whole annulus aeroelasticity analysis of a 17-bladerow WRF compressor using an unstructured Navier-Stokes solver," *Int. J. Comput. Fluid Dyn.*, **19**, 211–223 (2005).

[7] E. Envia, A. G. Wilson and D. L. Huff, "Fan noise: A challenge to CAA," *Int. J. Comput. Fluid Dyn.*, **18**, 471–480 (2004).

[8] D. J. Bodony and S. K. Lele "On the current status of jet noise predictions using large-eddy simulation," *AIAA J.*, **46**, 364–380 (2008).

[9] A. D. Pierce, "Wave equation for sound in fluids with unsteady inhomogeneous flow," *J. Acoust. Soc. Am.*, **87**, 2292–2299 (1990).

[10] M. K. Myers, "On the acoustic boundary condition in the presence of flow," *J. Sound Vib.*, **71**, 429–434 (1980).

[11] W. Eversman, "The boundary condition at an impedance wall in a non-uniform duct with potential mean flow," *J. Sound Vib.*, **246**, 63–69 (2001).

[12] G. G. Vilenski and S. W. Rienstra, "On hydrodynamic and acoustic modes in a ducted shear flow with wall lining," *J. Fluid Mech.*, **583**, 45–70 (2007).

[13] S. W. Rienstra and G. G. Vilenski, "Spatial instability of boundary layer along impedance wall," *AIAA Paper 2008-2932* (2008).

[14] S. W. Rienstra, "Impedance models in time domain including the extended Helmholtz resonator model," *AIAA Paper 2006-2686* (2006).

[15] C. K. W. Tam and L. Auriault, "Time domain impedance boundary conditions for computational aeroacoustics," *AIAA J.*, **34**, 917–923 (1996).

[16] K. Y. Fung, H. Ju and B. Tallapragada, "Impedance and its time-domain extensions," *AIAA J.*, **38**, 30–38 (2000).

[17] Y. Özyörük and L. N. Long, "A time-domain implementation of surface acoustic impedance condition with and without flow," *J. Comput. Acoust.*, **5**, 277–296 (1997).

[18] L. Sbardella, B. J. Tester and M. Imregun, "A time-domain method for the prediction of sound attenuation in lined ducts," *J. Sound Vib.*, **293**, 379–396 (2001).

[19] K. Y. Fung and H. Ju, "Time domain impedance boundary conditions for computational acoustics and aeroacoustics," *Int. J. Comput. Fluid Dyn.*, **18**, 503–511 (2004).

[20] C. Richter and F. H. Thiele, "The stability of time explicit impedance models," *AIAA Paper 2007-3538* (2007).

[21] K. W. Thompson, "Time dependent boundary conditions for hyperbolic systems, II," *J. Comput. Phys.*, **89**, 439–461 (1990).

[22] M. B. Giles, "Non-reflecting boundary conditions for Euler equation calculations," *AIAA J.*, **28**, 2050–2058 (1990).

[23] T. J. Poinsot and S. K. Lele, "Boundary conditions for direct simulations of compressible viscous flows," *J. Comput. Phys.*, **101**, 104–129 (1992).
[24] R. Hixon, "Radiation and wall boundary conditions for computational acoustics: A review," *Int. J. Comput. Fluid Dyn.*, **18**, 523–531 (2004).
[25] R. J. Astley, G. J. Macaulay, J.-P. Coyette and L. Cremers, "Three dimensional wave-envelope elements of variable order for acoustic radiation and scattering. Part I. Formulation in the frequency domain," *J. Acoust. Soc. Am.*, **103**, 49–63 (1998).
[26] W. Eversman, "Mapped infinite wave envelope elements for acoustic radiation in a uniformly moving medium," *J. Sound. Vib.*, **224**, 665–687 (1999).
[27] C. H. Wilcox, "A generalization of theorems of Rellich and Atkinson," *Proc. Am. Math. Soc.*, **7**, 271–276 (1956).
[28] B. Van Antwerpen, R. Leneveu and S. Caro, "New advances in the use of ACTRAN/TM for nacelle simulations," *AIAA Paper 2008-2827* (2008).
[29] J. A. Hamilton and R. J. Astley, "Acoustic propagation on irrotational mean flows using transient finite end infinite elements," *AIAA J.*, **43**, 124–134 (2005).
[30] F. Q. Hu, "Absorbing boundary conditions," *Int. J. Comput. Fluid Dyn.*, **18**, 513–522 (2004).
[31] J-P. Berenger, "A perfectly matched layer for the absorbtion of electromagnetic waves," *J. Comput. Phys.*, **114**, 185–200 (1994).
[32] J. W. Goodrich, "A comparison of three PML treatments for CAA (and CFD)," *AIAA Paper 2008-2922* (2008).
[33] F. Q. Hu, "A stable perfectly matched layer for linearized Euler equations in unsplit physical variables," *J. Comput. Phys.*, **173**, 455–480 (2001).
[34] S. K. Richards, X. Zhang, X. X. Chen and P. A. Nelson, "The evaluation of non-reflecting boundary conditions for duct acoustic computation," *J. Sound Vib.*, **270**, 539–557 (2004).
[35] P. G. Drazin and W. H. Reid, *Hydrodynamic Stability* (Cambridge University Press, Cambridge, 1981).
[36] A. Michalke, "On spatially growing disturbances in an inviscid shear layer," *J. Fluid Mech.*, **23**, 521–544 (1965).
[37] J. Manera, B. Schiltz, R. Leneveu, S. Caro, J. Jacqmot and S. Rienstra, "Kelvin Helmholtz instabilities occurring at a nacelle exhaust," *AIAA Paper 2008-2883* (2008).
[38] A. Agarwal, P. J. Morris and R. Mani, "Calculation of sound propagation in nonuniform flows: suppression of instability waves," *AIAA J.*, **42**, 80–88 (2004).
[39] C. Bailly and D. Juvé, "Numerical solution of acoustic propagation problems using linearized Euler equations," *AIAA J.*, **38**, 22–29 (2000).
[40] C. Bogey, C. Bailly and D. Juvé, "Computation of flow noise using source terms in linearized Euler's equations," *AIAA J.*, **40**, 235–243 (2002).
[41] R. Ewert and W. Schröder, "Acoustic perturbation equations based on flow decomposition via source filtering," *J. Comput. Phys.*, **188**, 365–398 (2003).
[42] X. Huang, X. Chen, Z. Ma and X. Zhang, "Efficient computation of spinning modal radiation through an engine bypass duct," *AIAA J.*, **46**, 1413–1423 (2008).
[43] B. J. Tester, Y. Özyörük and G. Gabard, "Influence of mean flow gradients on fan exhaust noise predictions," *AIAA Paper 2008-2825* (2008).
[44] F. Farassat and M. K. Myers, "Extension of Kirchhoff's formula to radiation from moving surfaces," *J. Sound Vib.*, **123**, 451–460 (1988).
[45] F. Farassat, "Linear acoustic formulas for the calculation of rotating blade noise," *AIAA J.*, **19**, 1122–1130 (1981).
[46] G. Ashcroft and X. Zhang, "Optimized prefactored compact schemes," *J. Comput. Phys.*, **190**, 459–477 (2003).
[47] S. W. Herrin, T. W. Wu and A. F. Seybert, "Boundary element modelling," in *Handbook of Noise and Vibration Control*, M. J. Crocker, Ed. (Wiley, New York, 2007), pp. 116–127.
[48] S. J. Horowitz, R. K. Sigman and B. T. Zinn, "An iterative finite element-integral element technique for predicting sound radiation from turbofan inlets in steady flight," *AIAA Paper 82-0124* (1982).
[49] M. H. Dunn, J. Tweed and F. Farassat, "The application of a boundary integral equation method to the prediction of ducted fan engine noise," *J. Sound Vib.*, **227**, 1019–1048 (1999).
[50] F. Montétagaud and S. Montoux, "Negatively scarfed intake: Design and acoustic pertformance," *AIAA Paper 2005-2944* (2005).
[51] D. Broszat, R. Maier and R. Pongratz, "Detailed analysis of the virtual scarf inlet (VSI) effect and performance," *AIAA Paper 2008-2980* (2008).
[52] A. Delnevo, S. Le Saint, G. Sylvand and I. Terrass, "Numerical methods: Fast multipole method for shielding effects," *AIAA Paper 2005-2971* (2005).
[53] G. Alleon, S. Champagneux, G. Chevalier, L. Giraud and G. Sylvand, "Parallel distributed numerical simulations in aeronautic applications," *Appl. Math. Model.*, **30**, 714–730 (2006).
[54] J. H. Lan, *Turbofan Duct Propagation Model* (NASA/CR-2001-211245, 2001).
[55] D. M. Nark, F. Farassat, D. S. Pope and V. Vatsa, "The development of the ducted fan noise propagation and radiation code CDUCT-LARC," *AIAA Paper 2003-3242* (2003).
[56] D. M. Nark and F. Farassat, "CDUCT-LaRC status — Shear layer refraction and noise radiation," *AIAA Paper 2006-2587* (2006).
[57] R. J. Astley and W. Eversman, "Finite element formulations for acoustical radiation," *J. Sound Vib.*, **88**, 47–64 (1983).
[58] R. J. Astley, "A finite element, wave envelope element formulation for acoustical radiation in moving flows," *J. Sound Vib.*, **103**, 471–485 (1985).
[59] A. V. Parrett and W. Eversman, "Wave envelope and finite element approximations for turbofan noise radiation in flight," *AIAA J.*, **24**, 753–760 (1986).
[60] G. Gabard, R. J. Astley and M. Ben Tahar, "Stability and accuracy of finite element methods for flow acoustics: I. General theory and application to one-dimensional propagation," *Int. J. Numer. Methods Eng.*, **63**, 947–973 (2005).
[61] G. Gabard, R. J. Astley and M. Ben Tahar, "Stability and accuracy of finite element methods for flow acoustics: II. Two-dimensional effects," *Int. J. Numer. Methods Eng.*, **63**, 974–987 (2005).
[62] D. Stanescu, D. Ait-Ali-Yahia, W. G. Habashi and M. P. Robichaud, "Spectral element method for linear fan tone noise radiation," *AIAA J.*, **42**, 696–705 (2004).
[63] E. Listerud and W. Eversman, "Finite element modeling of acoustics using higher order elements. Part II: Turbofan acoustic radiation," *J. Comput. Acoust.*, **12**, 431–446 (2004).
[64] W. Eversman and D. Obuknor, "Aft fan duct radiation," *J. Sound Vib.*, **213**, 235–257 (1998).
[65] Mumps: a multifrontal massively parallel sparse direct solver. *http://graal.ens-lyon.fr/MUMPS.*
[66] J. H. Lan and C. Breard, "Development and validation of a 3D linearized Euler solver," *AIAA Paper 2006-2585* (2006).
[67] N. Schoenwald, L. Panek, C. Richter and F. Thiele, "Investigation of sound radiation from a scarfed intake by CAA-FWH simulations using overset grids," *AIAA Paper 2007-3524* (2007).
[68] L. Panek, N. Schönwald, C. Richter and F. Thiele, "Simulation of the rearward propagation of fan noise through a long cowl

aero-engine," *AIAA Paper 2008-2820* (2008).
[69] M. Zhuang and R. F. Chen, "Application of high-order optimized upwind schemes for computational aeroacoustics," *AIAA J.*, **40**, 443–449 (2002).
[70] J. C. Kok, "Computation of sound radiation from cylindrical ducst with jets using a high order finite-volume method," *AIAA Paper 2007-3489* (2007).
[71] Y. Özyörük and S. Lidoine, "Numerical analysis of noise radiation from a turbofan exhaust cowl with an extended liner in flight," *AIAA Paper 2008-2880* (2008).
[72] R. Hixon, "A new class of comact schemes," *AIAA Paper 98-0367* (1998).
[73] X. Zhang, X. X. Chen, C. L. Morfey and P. A. Nelson, "Computation of spinning modal radiation from an unflanged duct," *AIAA J.*, **42**, 1795–1801 (2004).
[74] X. Zhang, X. X. Chen and C. L. Morfey, "Acoustic radiation from a semi-infinite duct with a subsonic jet," *Int. J. Aeroacoust.*, **4**, 169–184 (2005).
[75] S. K. Richards, X. X. Chen, X. Huang and X. Zhang, "Computation of fan noise radiation through an engine exhaust geometry with flow," *Int. J. Aeroacoust.*, **6**, 223–241 (2007).
[76] X. X. Chen, X. Huang and X. Zhang, "Sound radiation from a bypass duct with bifurcations," *AIAA J.*, **47**, 429–436 (2009).
[77] X. Huang, X. Zhang and S. K. Richards, "Adaptive mesh refinement computation of acoustic radiation from an engine intake," *Aerosp. Sci. Technol.*, **12**, 418–426 (2008).
[78] B. Cockburn, G. E. Karniadakis and C-W. Shu, *Discontinuous Galerkin Methods: Theory Computation and Applications*, Lecture Notes in Computational Science and Engineering, Vol. 11 (Springer-Verlag, Berlin, 2000).
[79] F. Bassi and S. Rebay, "High order accurate discontinuous finite element solution of the 2D Euler equations," *J. Comput. Phys.*, **138**, 251–285 (1997).
[80] H. L. Atkins and C. W. Shu, "Quadrature free implementation of the discontinuous Galerkin method for hyperbolic equations," *AIAA J.*, **36**, 775–782 (1998).
[81] D. Stanescu, M. Y. Hussaini and F. Farassat, "Aircraft engine noise scattering — A discontinuous spectral elememt approach," *AIAA Paper 2002-0800* (2002).
[82] P. P. Rao and P. J. Morris, "Application of a generalized quadrature free discontinuous Galerkin method in aeroacoustics," *AIAA Paper 2003-3120* (2003).
[83] N. Chevaugeon, J.-F. Remacle, X. Gallez, P. Ploumhans and S. Caro, "Efficient discontinuous Galerkin methods for solving acoustic problems," *AIAA Paper 2005-2823* (2005).
[84] F. Q. Hu and H. L. Atkins, "Two-dimensional wave analysis of the discontinuous Galerkin method with non-uniform grids and boundary conditions," *AIAA Paper 2002-2514* (2002).
[85] Y. Reymen, M. Baelmans and W. Desmet, "On the performance of the quadrature-free discontinuous Galerkin method on hexahedral and tetrahedral grids for linearized Euler equations," *AIAA Paper 2008-2301* (2008).
[86] R. Leneveu, B. Schiltz, S. Laldjee and S. Caro, "Performance of a DGM scheme for LEE and applications to aircraft engine exhaust noise," *AIAA Paper 2008-2884* (2008).
[87] Y. Zhao and P. J. Morris, "The prediction of fan exhaust noise propagation," *AIAA Paper 2005-2815* (2005).
[88] S. Redonnet, C. Mincu and E. Manoha, "Computational aeroacoustics of realistic co-axial engines," *AIAA Paper 2008-2826* (2008).
[89] D. Casalino, M. Roger and M. C. Jacob, "Prediction of sound proapagtion in ducted potential flows using Green's function disrcetization," *AIAA J.*, **42**, 736–744 (2004).
[90] P. Gamallo and R. J. Astley, "The partition of unity finite element method for short wave acoustic propagation on non-uniform potential flows," *Int. J. Numer. Methods Eng.*, **65**, 425–444 (2006).
[91] G. Gabard, "Discontinuous Galerkin methods with plane waves for time harmonic problems," *J. Comput. Phys.*, **225**, 1961–1984 (2007).
[92] G. F. Homicz and J. A. Lordi, "A note on the radiative directivity patterns of duct acoustic modes," *J. Sound Vib.*, **41**, 283–290 (1975).
[93] R. M. Munt, "The interaction of sound with a subsonic jet issuing from a semi-infinite cylindrical pipe," *J. Fluid Mech.*, **83**, 609–640 (1977).
[94] G. Gabard and R. J. Astley, "Theoretical model for sound radiation from annular jet pipes: Far- and near-field solutions," *J. Fluid Mech.*, **549**, 315–341 (2006).
[95] R. J. Astley, J. A. Hamilton, N. Baker and E. H. Kitchen, "Modelling tone propagation from turbofan inlets — The effect of extended lip iners," *AIAA Paper 2002-2449* (2002).
[96] B. J. Tester, F. Arnold, S. Caro and S. Lidoine, *Turbomachinery Noise Radiation through the Engine Exhaust: Project No. 516079, 6th Framework Programme: Publishable final activity report* (TURNEX Deliverable D0-1-9a 2008).

R. Jeremy Astley received a BSc(hons) degree in mathematics from the University of Canterbury in New Zealand in 1968 and MSc and PhD degrees in applied mathematics from Bristol University in the United Kingdom in 1970 and 1973. In 1999 he was awarded a higher doctorate (Doctor of Engineering) from the University of Canterbury for contributions to computational acoustics. He is currently Professor of Computational Aero-acoustics at the Institute of Sound and Vibration Research at the University of Southampton in the United Kingdom, and Director of the Rolls-Royce University Technology Centre in Gas Turbine Noise. He is a fellow of the Academy of the Royal Society of New Zealand (FRSNZ), a fellow of the Institution of Professional Engineers of New Zealand (FIPENZ) and a fellow of the international Institute for Acoustics and Vibration (FIIAV).